Applied Clay Science 47 (2010) 330–342

Contents lists available at ScienceDirect

Applied Clay Science

journal homepage: www.elsevier.com/locate/clay

3D-microstructure analysis of hydrated bentonite with cryo-stabilized pore water

L. Holzer [a,*], B. Münch [a], M. Rizzi [b], R. Wepf [c], P. Marschall [d], T. Graule [a]

[a] EMPA, Materials Science and Technology, Laboratory for High Performance Ceramics, 8400 Duebendorf, Switzerland
[b] EPFL, Ecole Polytechnique Fédérale, ENAC, Soil Mechanics Laboratory, 1015 Lausanne, Switzerland
[c] ETHZ, Swiss Federal Institute of Technology, EMEZ, Centre for Imaging Science and Technology, 8093 Zürich, Switzerland
[d] Nagra, National Cooperative for the Disposal of Radioactive Waste, 5430 Wettingen, Switzerland

ARTICLE INFO

Article history:
Received 26 January 2009
Received in revised form 4 November 2009
Accepted 23 November 2009
Available online 30 November 2009

Keywords:
Bentonite
Pore size distribution
Free water
Cryo
Focused ion beam (FIB)
Nanotomography

ABSTRACT

In saturated bentonite, free water is hosted in the meso- and macropores. Microscopic characterization of free water and the associated pore structure is very difficult because of the swelling- and shrinking-behaviour of montmorillonite. In this article, we present state of the art cryo-preparation techniques including high pressure freezing and low temperature freeze substitution, which enable the stabilization of bentonite microstructures. Microscopic analyses of cryo-stabilized bentonite samples are then performed with conventional SEM, with cryo-SEM and with FIB-nanotomography. From the resulting 2D- and 3D-images, so-called "continuous pore size distributions" are calculated and the 3D-connectivities of the mesopores are documented. Furthermore, from the comparison with pore size analyses that are based on conventional preparation techniques (oven drying and freeze drying), it is shown that high pressure freezing leads to more reliable results. Overall, it is demonstrated that reliable quantitative 3D-characterization can be achieved from the bentonite pore structure when high resolution 3D-imaging by FIB-nanotomography is combined with modern cryo-preparation techniques (i.e. high pressure freezing).

1. Introduction

Bentonite is a natural material which contains a high proportion of swelling clays (smectite). Due to the high water adsorption and ion exchange capacities, bentonite can be used in many different technological applications, e.g. catalysts in chemical and oil processing industries, admixtures for plastification and manipulation of viscosity of ceramic pastes or sealing materials for civil and environmental engineering. Compacted bentonite is characterized by low permeability, long-term stability, self-sealing capability and high adsorption capacity (Ito, 2006). Due to these properties, it is particularly well suited for barrier systems in nuclear waste repositories. For the long-term prediction of such repositories, it is of major interest to understand the relationship between the pore structure and the transport properties of dissolved radionuclides. Unfortunately, characterization of the multi-scale pore structure in hydrated and compacted bentonite is a difficult task. The microstructure continuously changes during hydration, swelling and compaction processes (Saiyouri et al., 2000). Therefore, it is difficult to prepare homogeneous bentonite samples with defined densities and water contents. In addition, conventional pore characterization methods such as mercury intrusion porosimetry (MIP), nitrogen sorption (BET) and electron microscopy (SEM / TEM) only work with dried materials (Delage et al., 2006). However, conventional drying techniques induce significant capillary forces which may lead to drying shrinkage artifacts. Therefore, it is a fundamental prerequisite for any microstructure investigation of hydrated bentonite to develop artifact-free sample preparation techniques.

Because of these difficulties, very little microstructural data are available which enable reliable quantitative descriptions of the pore structure in compacted bentonite. From a theoretical point of view, three different types of pores are generally distinguished depending on the physico-chemical properties of the pore water (Gimmi, 2003). The meso- and macropores mainly contain free pore water which is charge-balanced. In contrast the water in nanoscale pores is influenced by the surface forces which are essentially electrostatic in origin (Israelachvili, 1991). This bound water can further be classified into internal layers within the clay particles and external diffuse double layers (DDL) on the surface of the clay particles and other minerals. These three types of pore water have very different diffusional properties. For the understanding of diffusion in bentonite it is therefore of major interest to quantify the proportions of the different pore water types. These proportions are usually determined by indirect methods, e.g. by means of structural transport modelling (Appelo, 2008). Today, the reported proportions and especially the amount of free pore water in compacted bentonite are subject of a controversial debate which underlines the necessity to develop suitable techniques for reliable quantification of the pore structure in materials with swelling clays.

* Corresponding author. EMPA, Materials Science and Technology, Ueberlandstrasse 129, Laboratory for High Performance Ceramics (123), 8400 Duebendorf, Switzerland. Tel.: +41 44 823 44 90; fax: +41 44 823 41 60.
E-mail address: lorenz.holzer@empa.ch (L. Holzer).

0169-1317/$ – see front matter © 2009 Elsevier B.V. All rights reserved.
doi:10.1016/j.clay.2009.11.045

As an alternative to the conventional drying techniques, cryo-preparation can be used to stabilize the microstructure of hydrous materials. In a first cryo-SEM study of hydrated bentonite, the structure of the large-scale pores was investigated (Delage et al., 1982). Furthermore plunge freezing in liquid nitrogen (Chenu and Tessier, 1995) and also propane jet-freezing has been applied in combination with cryo-SEM for microstructural characterization of hydrated clays (Smart et al., 2004). However, plunge freezing of water-rich samples is only suitable for samples with a maximum thickness of 5 µm. In larger samples, freezing artifacts related to uncontrolled growth of large ice crystals may occur during plunge freezing due to the sluggish heat conduction of water and clay. Fortunately, more sophisticated cryo-techniques based on high pressure freezing are available nowadays which are used e.g. in life-sciences for the preservation of functional hydrated states and native molecular arrangements. Thereby the formation of ice crystals is strongly suppressed at pressures of 2 kbar. With these methods also the pore water in mineralogical materials can be vitrified within a few milliseconds. Details of the high pressure freezing technique and the corresponding laws of low temperature physics are discussed in Bachmann and Mayer (1987). For the present study, we have adapted the high pressure freezing method for the investigation of hydrated bentonites.

Instead of investigating the high pressure frozen samples by means of cryo-microscopy, the cryo-samples can be impregnated by freeze substitution and then analyzed with conventional microscopy techniques. Thereby the frozen water is replaced gradually by organic solvents and subsequently the samples are impregnated at low temperatures with epoxy resin. New freeze substitution protocols are available which open exciting possibilities for correlative, multimodal imaging at different length scales (CLSM, SEM, TEM, X-ray CT) (Biel et al., 2003; Wepf, 2007). For the analysis of multi-scale pore structures, correlative microscopy in combination with freeze substitution represents an interesting option which may help to obtain a more consistent picture of the complex bentonite microstructures. Alternatively, Transmission X-ray microscopy (TXM) which is a new synchrotron based technique allows direct investigation of the microstructure in hydrated clays (Zbik et al., 2008) without drying or stabilizing the samples. However, since TXM is still limited to a resolution of approximately 100 nm voxel size, for quantitative analysis of the pore structure in clay rich materials, this method needs further improvement of resolution and contrast.

For the correlation of microstructural features with the corresponding transport properties, various topological parameters have to be taken into account. Simple pore volume fractions can be obtained already from 2D images. However, higher order topological parameters such as connectivity, tortuosity and constrictivity are more relevant for the link with transport properties. These parameters can only be extracted from 3D images. In this context focused ion beam-nanotomography (FIB-nt) opens new possibilities for the investigation of 3D pore structures at sub-µm scales. Details of the 3D-FIB technique which is based on high resolution serial sectioning are given in Holzer et al. (2004). In recent years, this method was successfully applied in numerous investigations for the characterization of 3D microstructures in ceramic, metallic and composite materials (Holzapfel et al., 2007; Holzer et al., 2006a; 2006b; 2006c; 2007; Inkson et al., 2001; Konrad et al., 2006; Kubis et al., 2004; Lasagni et al., 2006; 2008; Münch et al., 2006; Uchic et al., 2006; Wilson et al., 2006; Zaafarani et al., 2006). With FIB-nt voxel resolutions in the range of 10 nm can be reached, which enables the investigation of meso- and macropores in bentonite. Such 3D pore structures are often described with pore size distribution functions. For this purpose special algorithms for determination of so-called continuous pore size distributions (PSD) were developed. The new geometrical concept allows reliable statistical analyses of networked pore structures which are compatible with the results from physical experiments such as mercury intrusion porosimetry (Münch and Holzer, 2008).

In the present study, the pore structure of hydrated bentonite is investigated with state of the art methods including cryo-preparation, high resolution 3D-imaging with FIB-nt and quantification based on continuous PSD algorithms. Special emphasis is placed on a quantitative comparison of conventional sample preparation techniques (oven drying and plunge freeze drying) with high pressure freezing and freeze substitution. This comparison is performed on a water-rich bentonite paste. In a second step, cryo-techniques and FIB-nt are used for the investigation of the pore structure in compacted bentonite. Thereby, the meso- and macropores which contain the free pore water are described with continuous PSDs and their 3D-connectivity is illustrated qualitatively.

2. Materials

In this study, the mesoscopic pore structures of two bentonite materials (Ben I and Ben IV) are investigated. They both consist of commercial Bentonite MX80 (CETCO Company) which contains approximately 80% montmorillonite and 20% accessory minerals. Detailed mineralogical descriptions of bentonite MX80 are given elsewhere (Karnland et al., 2006).

The proportions of the initial mix of the samples Ben I and Ben IV are given in Table 1. Ben I is a mixture of 31.2 wt.% of dry bentonite with 68.8 wt.% of water. The corresponding gravimetric water content with respect to the dry weight is 220%, which represents the percentage of the weight of water relative to the weight of the solid particles. Ben I is an uncompacted material which has a high amount of free water even after hydration and incorporation of water into the clay interlayers. It has a dry density of 0.39 kg/m^3.

Ben IV is a compacted material which has much lower water content than Ben I (mixture of 21.5 wt.% H_2O and 78.5% dry bentonite, which corresponds to a water content of 27.4%). Consequently it has a higher dry density (1.58 kg/m^3). The water content in the initial mix was calculated so that it would be sufficient for complete saturation of the clay interlayers. After saturation, only a few % of free water are expected in Ben IV. The sample Ben IV was produced by compacting in an oedometric cell a defined amount of material to the desired initial dry density by means of a uniaxial load of about 25 MPa. The weight of the bentonite required in order to manufacture the specimen was calculated taking into account the volume of the compaction mould and the desired initial density. The mix was prepared by starting from the granular material at equilibrium with laboratory conditions, sieving it at 0.5 mm, and finally adding in a stepwise way the exact amount of water, in order to make a homogeneous mixture. It was then allowed to mature for 24 h. This material was afterwards compacted to the calculated volume which results in a density of 1.58 kg/m^3. After compaction the sample was cut into two halves, one devoted to the microstructural analysis and the other to the measurements of the initial water content, saturation degree, and dry density by means of an advanced pycnometer method which uses kerdane as filling liquid (Peron et al., 2007). The measured degree of saturation in Ben IV is equal to 96%, which indicates that some air was trapped in a few voids. Despite these minor imperfections the sample can be considered as nearly saturated.

3. Methods

For the microscopic investigation of free water and of the associated pore structure in hydrated bentonite, the microstructure

Table 1
Mixing proportions of dry bentonite (MX80) and water.

Sample name	wt.% of water	vol.% of water	Saturation	Dry density [kg/m^3]
Ben I	68.8	85.6	100%	0.39
Ben IV	21.5	42.4	96%	1.58

of the initially wet material has to be stabilized with suitable preparation methods. In this study, four different sample preparation techniques were applied in order to test their suitability for bentonite investigations or alternatively to identify possible artifacts. The four preparation techniques are:

- Oven drying (OV)
- Plunge freezing and freeze drying (FD)
- High pressure freezing and freeze fracturing (HPF–FF)
- High pressure freezing and controlled freeze drying (HPF–FD)

Subsequently, microscopic investigations were carried out with ESEM for 2D-analysis, with focused ion beam-nanotomography (FIB-nt) for 3D-characterization and with cryo-SEM for investigations of freeze-fractured samples (HPF–FF). The microscopic procedures and the image analysis techniques for quantification of the pore size distributions (PSD) are described below in Sections 3.2 and 3.3.

3.1. SEM-preparation / stabilization of the microstructure

3.1.1. Oven drying (OV)

Small pieces (cylinders: 3 mm in diameter, 5 mm height) of wet material (Ben I and Ben IV) were dried in a furnace at 110 °C for 24 h. After drying, the samples were stored in a desiccator for thermal equilibration with ambient conditions. In numerous clay studies, this dried material is then used for mercury porosimetry (MIP) and for nitrogen sorption/desorption analysis (BET), regardless of the possible artifacts, which shall be investigated here by microscopy techniques. For microscopic investigations with backscattered electrons (BSE), the samples have to be impregnated, ground and polished. Impregnation is preformed under vacuum with a low viscosity epoxy resin (4 parts Araldit BY158 and 1 part Aradur 21, www.huntsman.com). In order to improve the impregnation of small pores, the samples are stored for 12 h in a pressure chamber during the hardening of the epoxy. Grinding and polishing with an oil-based diamond suspension (automet, www.buehler.com) were carried out according to standard sample preparation procedures for SEM (Crumbie, 2001). The samples were then coated with a thin carbon-film for BSE-imaging in (E)SEM. Alternatively, the samples were covered with a thick Pt-coating before cross-sectioning with FIB.

3.1.2. Plunge freezing and freeze drying (FD)

During conventional drying, capillary forces may induce drying shrinkage. During freeze drying water is sublimated from a frozen state and hence no capillary forces occur. For this purpose, small pieces (3 mm in diameter) of wet material (Ben I and Ben IV) were frozen in liquid nitrogen (boiling point −196 °C). Freeze drying was then performed with the apparatus ALPHA 1–4 LSC from Christ (www.martinchrist.de). The samples were stored at pressures below 10^{-3} mbar for 14 days. After 14 days in the freeze dryer, the sample weight remained constant. In this dry state, the material can also be used for MIP and BET analyses. For SEM- and FIB-investigations the dried material had to be impregnated and polished in the same way as described above for the oven dried samples.

Formation of ice crystals during plunge freezing bears a certain potential for artifacts. Furthermore in the freeze drying process, the temperatures are not controlled with a specific cooling unit in the freeze drying apparatus ALPHA. The samples are cooled only by the endothermal sublimation of the frozen water. During the ongoing drying process the reaction rates gradually decrease and the samples start to re-equilibrate with ambient temperatures. These uncontrolled temperature changes may lead to a recrystallization of the remaining frozen water, which can also lead to microstructural changes.

3.1.3. High pressure freezing and freeze fracturing for Cryo-SEM (HPF–FF)

Formation of ice crystals can be suppressed with high pressure freezing which is performed with a HPM 010 apparatus (Leica/Bal-Tec, www.bal-tec.com). The wet samples are placed between two aluminium specimen carriers (type A) from Leica (Leica Microsystems, Vienna, A). The cylindrical cavity of the sample holders has dimensions of 2 mm (diameter) and 400 µm (thickness). The high pressure frozen samples are then fractured under liquid nitrogen or under high vacuum, etched for 5 min at −110 ° C and unidirectionally coated with 2 nm W at an elevation angle of 45°. Furthermore, the surface structure is stabilized for SEM imaging with an additional layer of 2 nm W under changing elevation angle from 10° to 90° during deposition in a BAF 060 apparatus (Leica/Bal-Tec). The samples are transferred to the cryo-microscope with a VCT 100 system (Leica/BAL-TEC). The Cryo-SEM investigations are then performed with a Zeiss Gemini 1530 FEG microscope. This SEM is equipped with a cryo-stage which is set to temperatures of −120 °C during observation of the samples. All cryo-preparations and -investigations are performed at the centre for electron microscopy at ETH Zürich (EMEZ).

3.1.4. High pressure freezing and controlled freeze drying (HPF–FD)

In order to investigate high pressure frozen samples in conventional SEM and FIB, the frozen samples have to be dried and infiltrated with a resin. In contrast to the conventional freeze drying (as described above for plunge frozen samples), the HPF samples are freeze dried under controlled temperature conditions in order to prevent the frozen water from recrystallization. After high pressure freezing in a HPM 010 apparatus, controlled freeze drying is performed in a BAF 400 apparatus in five steps with decreasing temperatures (−110 °C / 2 h, −100 °C / 2 h, −80 °C / 2 h, −50 °C / 1 h and 4 °C / 1 h). The completely dehydrated HPF samples are withdrawn from the vacuum under a dry nitrogen atmosphere and submerged in the monomer-solution of a low viscosity resin (Epon-Durcupan ACM, Epoxy-Resin set from Fluka SA) and infiltrated for at least 12 h at room temperatures. Polymerisation of the embedded material was performed during 48 h at 60 °C. In this way, the small samples are embedded in a hard polymer which is suitable for microtome preparation. Block faces with planar surfaces are obtained by water free cross-sectioning with a microtome (Ultracut E, Leica microsystems) and a diamond knife (Diatome SA, Switzerland). For subsequent SEM- and FIB-imaging, the blockfaces are then mounted on an Al-stub and coated with C and Pt, respectively. It has to be noted that freeze drying can also be applied to freeze-fractured samples which have been investigated in cryo-SEM previously. In this way, a high pressure frozen sample can be investigated first with cryo-SEM (freeze fractured) and afterwards with high vacuum SEM or FIB (freeze dried and impregnated).

3.2. Microscopy techniques: ESEM, FIB-nt and Cryo-SEM

3.2.1. Back-scatter electron imaging (BSE) in ESEM

2D-images of impregnated and polished samples from Ben I (OV, FD, HPF–FD) are obtained with an environmental scanning electron microscope ESEM XL30 FEG from FEI which is equipped with a 4 quadrant solid state BSE-detector. The investigations are performed under high vacuum with accelerating voltages between 10 to 15 kV and with spot size 3.

3.2.2. Focused ion beam-nanotomography (FIB-nt)

FIB-nt analyses of high pressure frozen and freeze dried samples (HPF–FD) from Ben I and Ben IV are performed with a DualBeam FIB StrataDB235 from FEI. For 3D analysis at high resolutions (i.e. voxel size <20 nm), an automated serial sectioning procedure with integrated drift correction has been developed. Details of the FIB-nt procedures are described in previous publications (Holzer et al., 2004; Holzer et al., 2006c). FIB-nt of bentonite samples is performed with the in-lens detector (TLD-B) at 35,000× magnifications using accelerating voltages of 3 kV and spot size 3.

3.2.3. Cryo-SEM and in-situ sublimation

As described above, cryo-SEM investigations of high pressure frozen and freeze-fractured samples (HPF–FF) from Ben I and Ben IV are performed with a Zeiss Gemini 1530 FEG SEM which is equipped with a nitrogen-cooled cryo-stage. In the high vacuum of the cryo-SEM (10^{-6} mbar) the frozen water is stable at temperatures of −120 °C or below. Good imaging results are then obtained at 5 kV using the in-lens SE-detector. Nevertheless, in the dense microstructure of compacted bentonite (Ben IV) the distinction between pores with free water and solid clay is difficult. However, the water filled pores can be visualized by sublimating carefully the free water at slightly elevated temperatures (−80 °C) and by comparing the images from before and after sublimation. After sublimation, the formerly water filled pores will appear as dark holes. This in-situ sublimation is identical with the first steps of a controlled freeze drying process but with continuous observation of the microstructural changes.

3.3. Image analysis and quantification

For a better comparison of the different sample preparation techniques, the pore structures of the different samples have to be described quantitatively. In this context it is important to note that the results of any pore size measurement technique are strongly dependent on the geometrical definition of the pore size. Contrasting geometrical concepts of discrete and continuous pore size distributions (PSD) are defined elsewhere (Münch and Holzer, 2008). In the present study we are applying the concept of a continuous pore size distribution (PSD) which is geometrically related to the pore size perception of mercury intrusion porosimetry (MIP). In MIP the liquid mercury is pressed into the sample by increasing the pressure incrementally and thereby continuously filling smaller and smaller pores. For the measurement of a continuous PSD based on image data the mercury intrusion process is simulated. Thereby the intrusion process is not initiated at the sample boundaries (like in the real MIP experiment) but it is started from the pore locations which represent local maxima of the pore size. By incrementally reducing the radius of the intruding liquid, pores with lower dimensions can be filled successively. A 'continuous PSD' is then obtained by integration of the infiltrated volume over the corresponding range of radii. In contrast to real MIP, the simulated intrusion for continuous PSD measurement takes into account local maxima of pore size. In this way, the intrusion is performed along numerous but relatively short percolation chains which do not contain any pore necks (i.e. no local minima). Therefore the so-called ink bottle effect can be suppressed in the simulations. Under the assumption that the image data is representing the true pore structure of the sample, the continuous PSDs obtained from image modelling are more reliable than the size distributions from mercury porosimetry (MIP), because the latter are always affected by the ink bottle effect. The continuous PSD has also advantages compared to more conventional discrete PSDs that are usually obtained by image analysis. The discrete PSD considers the radii of area equivalent circles (in 2D) or of volume equivalent spheres (in 3D) for individual objects that can be identified as a pore in the image data. However, since the pore structure usually represents a continuous network, identification of discrete pore objects and determination of their respective sizes are ill defined. For continuously networked pore structures the measured discrete PSDs are strongly depending on imaging parameters (resolution, size of image window, orientation of imaging plane) and of the object recognition procedure (see e.g. Münch et al., 2006). Hence, for networked microstructures the continuous PSDs are more reliable than discrete PSDs. For more details on the geometrical principles of continuous and discrete PSDs we refer to a previous publication (Münch and Holzer, 2008), where mathematical definitions and illustrative examples are presented.

Very often segmentation is one of the most critical steps in image processing, because the corresponding results are strongly influenced by image imperfections and by poor contrast and resolution. Fortunately, the ESEM/BSE images of Ben I exhibit perfect contrast between pore and solid material and therefore segmentation by thresholding is accurate. The images from cryo-SEM also show a good contrast between clay flakes and the matrix of frozen water. However, since a majority of the clay flakes have a thickness of only 20 nm (see Fig. 5), small variations in the threshold level may lead to significant differences of the porosity measured from cryo-SEM images. In order to reduce these uncertainties the cryo-SEM images are taken at the highest possible resolution (i.e. with a pixel size of 3.7 nm at 100,000× magnification). The impact of the resolution is also studied by comparing results from images with different resolutions (see Figs. 1–6).

The concept of a continuous PSD can be applied to 2D-images (e.g. from ESEM) as well as to 3D-images (e.g. from FIB-nt). Nevertheless, an accurate 3D-analysis from a FIB-nt volume requires additional processing steps. First of all, spatial drifts in *x*- and *y*-directions, which occurred during the serial sectioning and the acquisition of the FIB/SEM images, have to be corrected. This is performed by successive alignment of any two subsequent images, by determination of the maxima of their 2D cross correlation functions at subpixel precision and by corresponding translation. Accordingly, image defects such as non-uniform illumination and waterfall effects (vertical stripes) have to be corrected. Non-uniform illumination and irregular background gray levels are caused mainly by the oblique SE-imaging angle of 52° in dual beam FIB. These defects are corrected by approximation of the background gray levels of the original images with second-order polynomial functions of the form: $B(x,y) = a_0 + a_1 \times x + a_2 \times y + a_3 \times x^2 + a_4 \times y^2 + a_5 \times xy$ (Russ, 1999). The so-called waterfall effect is caused by local variations in the sputtering and milling efficiency related to hard particles and soft pores. The resulting vertical stripes are corrected with combined wavelet and fast Fourier transform (FFT) filters (B. Münch, unpublished). After correction of these image defects, the 3D-data from FIB-nt is segmented by thresholding. The continuous PSDs are then calculated from these 3D pore structures. Finally, the surfaces of the pore structures are triangulated and visualized with the software Avizo 5.0 (Mercury Computer Systems, www.avizo3d.com).

Systematic differences must be expected when measuring PSDs from 2D- and from 3D-data. This must be considered when comparing results from ESEM (2D) and FIB-nt (3D). The differences between 2D- and 3D-continuous PSDs are explored by applying the PSD algorithms twice to the same stack of images from FIB-nt. In the first run, the PSD is extracted from the 3D-pore structure. In the second run, the PSDs are extracted from the single 2D-images. The 2D results are then averaged for the entire stack of images. In this way evidence is provided that the continuous PSDs from 2D-methods such as ESEM/BSE can be compared with the results from 3D image volumes from FIB-nanotomography.

4. Results

4.1. Microstructure of the water-rich sample Ben I

The hydrated sample Ben I contains a considerable amount of free water which is estimated to be 75 vol.% based on the initial mix proportions of dry bentonite with water and by taking into account the amount of water that is necessary for clay saturation. Due to the high amount of free water this sample exhibits a high potential for preparation artifacts which may arise either from drying shrinkage or from ice crystal growth during cryo-preparation. The water-rich material Ben I is therefore used to test the suitability of the different sample preparation techniques for microstructure analysis of hydrated bentonite. The resulting PSDs are compared with each other in

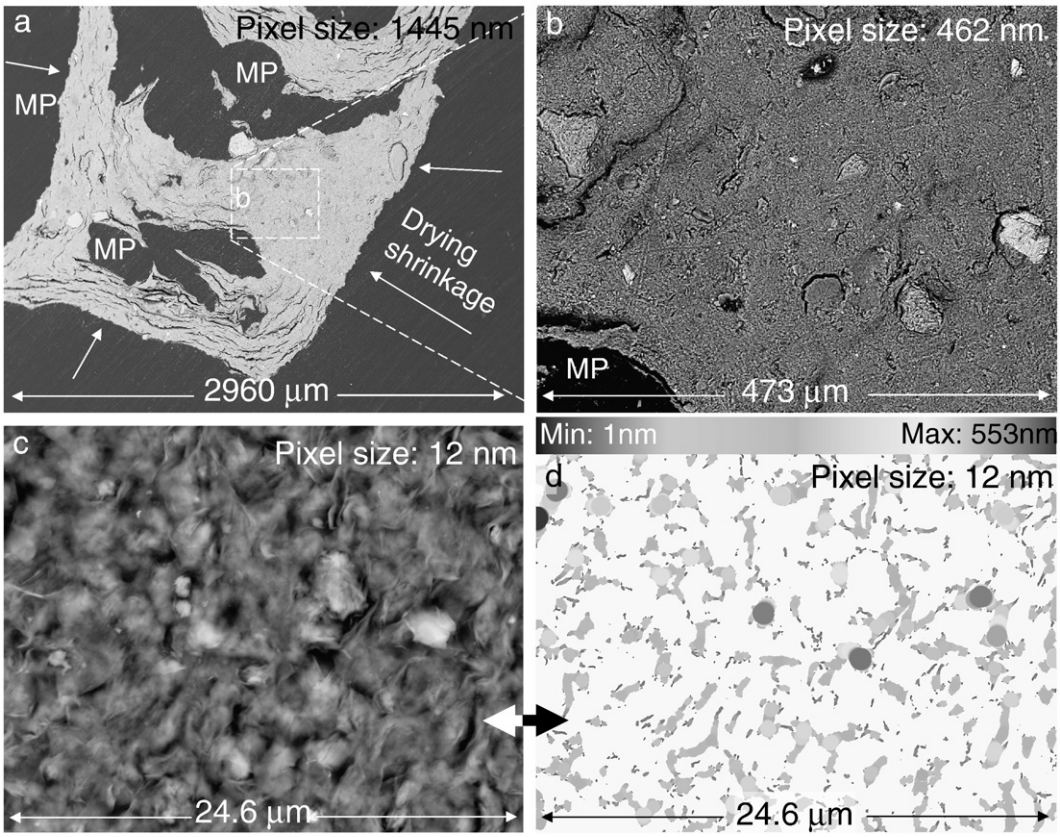

Fig. 1. ESEM/BSE images of oven dried sample Ben I OV at increasing magnifications (from a to c). At low magnifications (a) drying shrinkage of the entire sample and formation of macropores (MP) are apparent. Bottom right (d) is a gray-scale coded map of the pore size distribution in c. The corresponding PSD curve based on pixel resolution 12 nm and image width 24.6 µm is shown in Fig. 2.

order to identify and to quantify possible preparation artifacts. The most suitable sample preparation techniques are then selected for the investigation of the pore structure in the compacted bentonite sample Ben IV.

4.1.1. Oven drying

The ESEM images in Fig. 1 illustrate the microstructure of sample Ben I OV after drying at 110 °C. Already on a macroscopic scale it can be observed that the sample underwent drying shrinkage of approximately 50% from the initial sample volume. Macropores have formed at the mm-scale as a consequence of the shrinkage (Fig. 1a). The dried bentonite body itself is characterized by a dense and homogeneous microstructure (Fig. 1b and c). Based on the ESEM micrographs the pore size distributions in Ben I OV are calculated by applying the continuous PSD algorithms described in Münch and Holzer (2008). Fig. 1d illustrates the continuous PSD as a gray scale coded map. Thereby the intermediate pore sizes are bright gray (eg. 200–300 nm). The smallest pores (e.g. 1–20 nm) are shown in dark

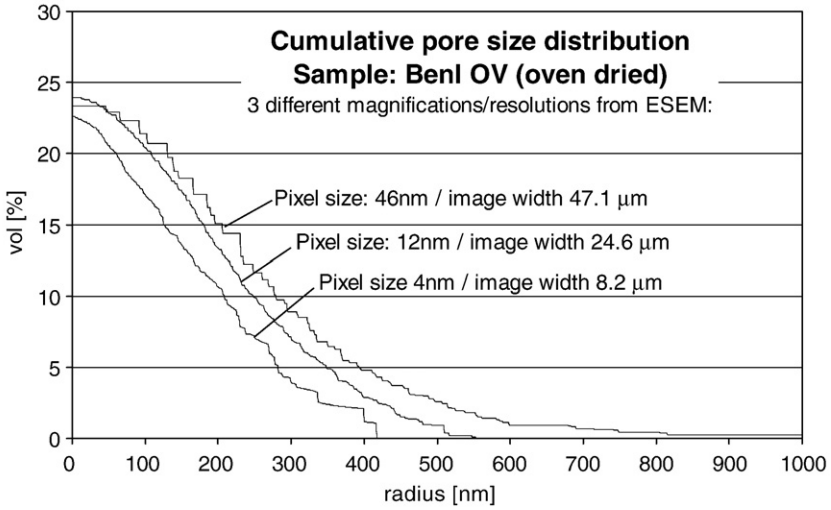

Fig. 2. Cumulative pore size distributions obtained from 3 different ESEM/BSE images of oven dried sample Ben I OV. The PSD measurements for different resolutions (4, 12 and 46 nm, respectively) give nearly identical results. Note: The pore volume has significantly decreased due to drying shrinkage from initially 75 vol.% in the bentonite mixture to 25 vol.% after oven drying.

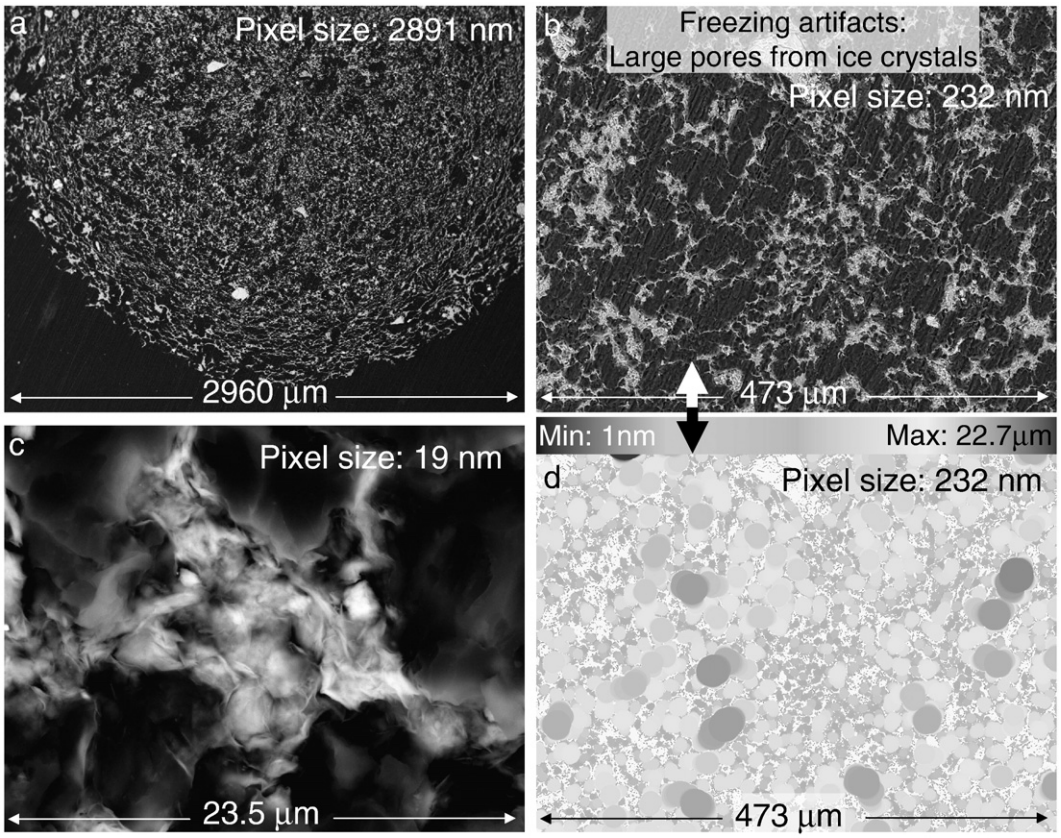

Fig. 3. ESEM/BSE images of freeze dried sample Ben I FD at increasing magnifications (from a to c). No shrinkage is apparent. However the eutectic microstructure indicates the presence of freezing artifacts due to the growth of large ice crystals. Bottom right (d) is a gray-scale coded map of the pore radii in b. The pore size distribution curve corresponding to the images in panels b/d (pixel resolution 232 nm / image width of 473 µm) is shown in Fig. 4.

gray as well as the largest pores (in the size range of 500 nm and larger). Fig. 2 shows the pore size distributions from three different ESEM images at pixel resolutions of 46 nm, 12 nm and 4 nm, respectively which correspond to image widths between 8.2 µm and 24.6 µm. The majority of the pores have characteristic radii between 100 and 400 nm. The three PSD curves are very similar to each other. This consistency confirms that the methodological reproducibility is satisfying. The main deviation in the PSDs from different magnifications is the perception of the maximum pore size for which the size of the image window is critical. The smaller the image window, the larger is the apparent maximum pore size. This effect can be attributed to the smaller field of view at higher magnifications which is insufficient for representative detection of the largest pores. The most significant feature of the oven dried sample, however, is that the total porosity has decreased from initially 75 vol.% to less than 25 vol.%. This reduction of macro- and mesopores is attributed to the drying shrinkage.

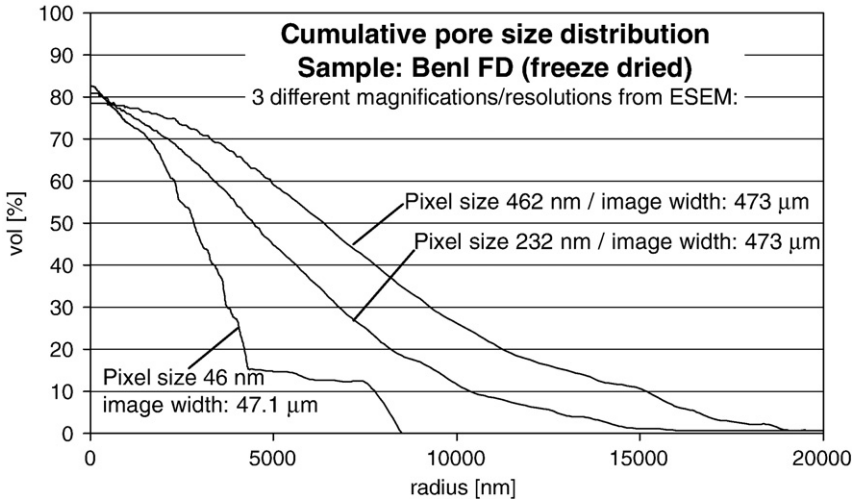

Fig. 4. Cumulative pore size distributions obtained from 3 different ESEM/BSE images of the freeze dried sample Ben I FD. The total porosity is close to 80 vol.% and the maximum pore radius is >20 µm. The irregular shape in the PSD curve at highest magnifications (46 nm) is attributed to the limited size of view (only 47 µm image width).

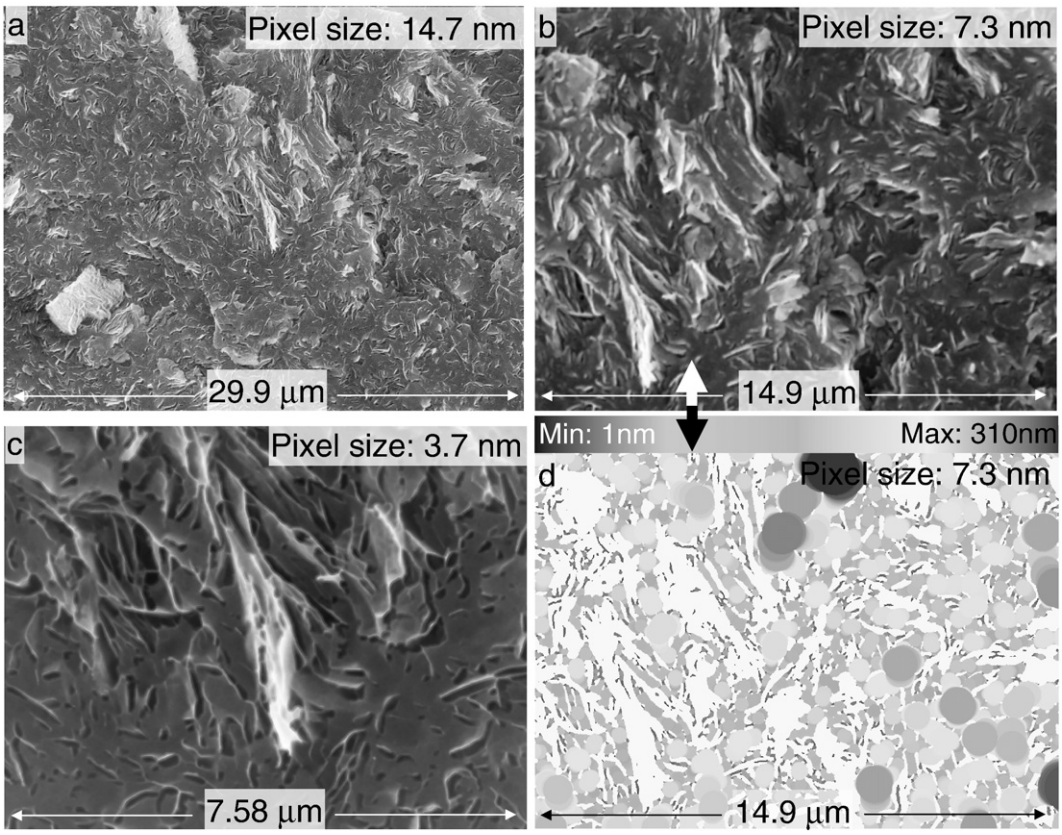

Fig. 5. Cryo-SEM images of a high pressure frozen and freeze-fractured sample Ben I HPF–FF at increasing magnifications (a–c). The images document that bentonite flakes (white) are well dispersed in the amorphous matrix of frozen water (dark gray). Bottom right (d) is a distance map of the water filled "pore space" in b. The corresponding pore size distribution curve "Pixel size: 7.3 nm" is shown in Fig. 6.

4.1.2. Freeze drying

In the freeze dried sample, no macroscopic shrinkage is observed (Fig. 3a). However, in contrast to the oven dried sample the freeze dried bentonite has a much coarser porosity. The clay particles form an interconnected network (Fig. 3b and c) which acts as an interstitial phase between the numerous coarse pores. This texture is characteristic for segregation patterns in plunge frozen suspensions. Thereby, the large pores represent pseudomorphs of the former ice crystals. The interstitial clay particles are forming a eutectic pattern which has accumulated between the ice crystals during plunge freezing. The colour coded distance map in Fig. 3d illustrates the pore size distribution which corresponds to the PSD curve "Pixel size: 232 nm" in Fig. 4. Note that the maximum pore radius is now larger than 20 µm. The total porosity in the freeze dried sample is 80 vol.% which is compatible with the estimation of free water in Ben I. The PSD curves show a wide size distribution from sub-µm scale up to 20 µm. Because of the coarse porosity, representative analyses can only be achieved at relatively low magnifications with corresponding large image widths of 473 µm. The PSD curve from high magnification image with high pixel resolution of 46 nm is clearly not representative. The limited field of view (image width only 47 µm) is not sufficient for statistical analysis of pores with diameters between 10 and 40 µm.

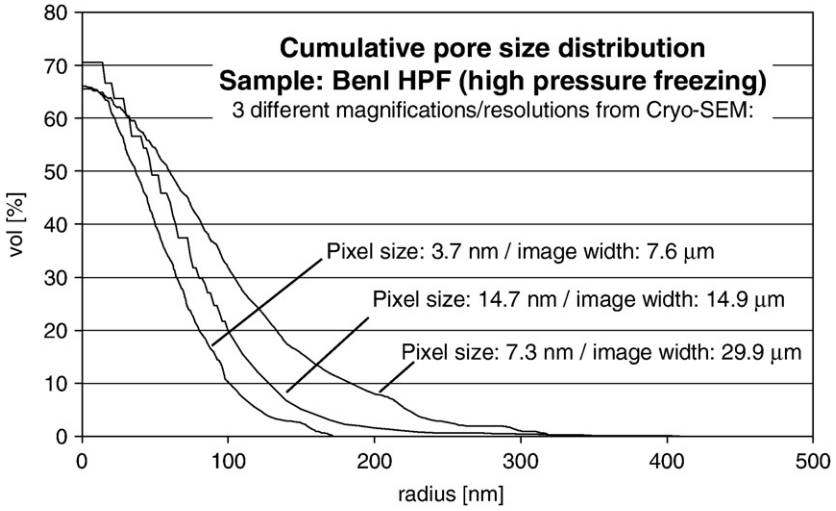

Fig. 6. Cumulative PSD curves obtained from cryo-SEM images of the high pressure frozen sample Ben I HPF–FF.

4.1.3. High pressure freezing and freeze fracturing

Cryo-SEM enables the investigation of hydrated material without removing the water from the sample. The microstructure of the high pressure frozen and freeze-fractured sample Ben I HPF–FF is shown in Fig. 5. Numerous small clay particles (white flakes) are uniformly dispersed in the amorphous matrix of frozen water (gray). No evidence for freeze segregation can be detected in this sample. Obviously growth of large ice crystals can be suppressed with high pressure freezing. The clay particles are much smaller than in the oven dried and freeze dried samples which underwent shrinkage or segregation. The thickness of the individual clay particles in high pressure frozen samples is typically in the range of 10 to 20 nm. Since the thickness of the individual TOT-layers in fully hydrated montmorillonite is approximately 22 Å (Saiyouri et al., 2000) the observed particle thickness corresponds to a stacking number of 5 to 10 clay layers. In contrast, the particles in the dry bentonite have thicknesses in the µm-range which corresponds to stacks with hundreds of clay layers. It is therefore assumed that the hydration of the clay particles in non-compacted bentonite is associated with extensive exfoliation and dispersion of thin clay layers. The pore size distributions in the high pressure frozen sample Ben I HPF–FF are shown in Fig. 6. Due to the dispersion of the numerous exfoliated clay particles, the pore structure is strongly fragmented and the pore radii are in the range of only 20 to 200 nm. In all measurements the total porosity is approximately 70 vol.% which is close to the estimated amount of free water. Hence, no evidence for freezing artifacts can be identified in the high pressure frozen sample.

It is important to note, that the maximum 'pore' size is much smaller (<0.2 µm) compared to the oven and freeze dried samples (up to 20 µm maximum pore size) and hence a much smaller field of view is required for representative analysis of the microstructure in the high pressure frozen sample. A comparison of PSDs from the differently dried samples is also shown in Fig. 9 (see discussion below).

4.1.4. High pressure freezing and controlled freeze drying

The filigree microstructure observed with cryo-SEM after high pressure freezing is carefully freeze dried in controlled temperature steps and then stabilized by infiltration with a low-viscous resin. The microstructure is then analyzed in 3D with FIB-nanotomography. As shown in 3D (Fig. 7), Ben I has a card house-type microstructure whereby the thin clay flakes form a grain-supported texture. In some locations, there exist some particles with increased thickness. Overall, the microstructure is homogeneous and uniform, which is compatible with the observations in cryo-SEM (Fig. 5). The pore size distributions are determined in 3D for the entire data volume (voxel dimensions 8.5 nm × 10.8 nm × 33 nm) and in 2D for individual images of the stack (pixel dimensions 8.5 nm × 10.8 nm). All PSD curves show size distributions with maxima between 100 and 200 nm (Fig. 8). Thereby, the PSD curves from 2D-analyses are systematically shifted to larger sizes compared to the PSD from 3D-analysis.

Intuitively one might expect that a 2D PSD would be smaller than a 3D PSD because of a higher chance to intersect an area smaller than the 'true pore size'. However, also the opposite case is possible. Thereby the 2D section may reveal an apparent pore size that is larger than the 'true pore size'. Thereby, the 'true pore size' of the continuous PSD is by the maximum size a sphere which can be placed into the 3D pore body at the specific location. For non-spherical or non-cylindrical objects with irregular shapes (such as elongated or oblate pore geometries) the maximum size of a circle (in 2D) that can be placed

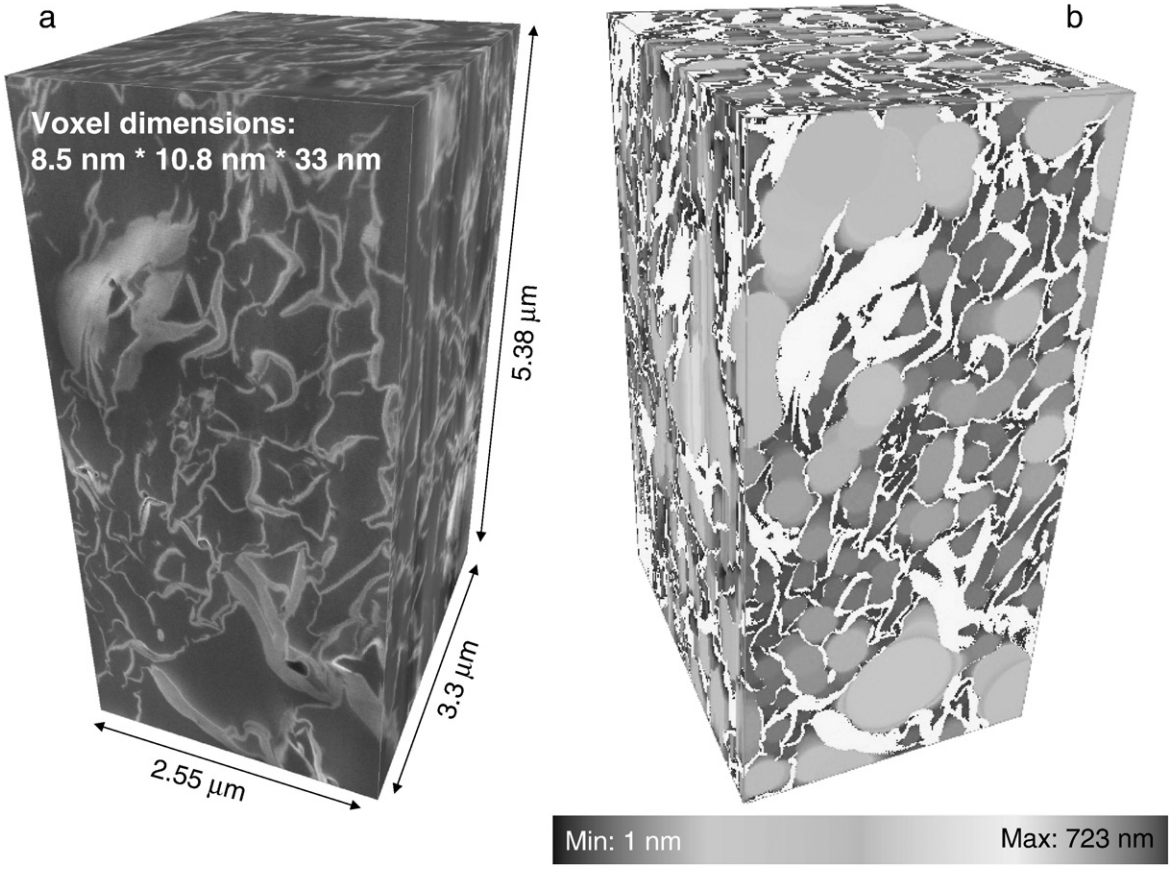

Fig. 7. 3D-microstructure of a high pressure frozen and freeze dried sample Ben I HPF–FD obtained from FIB-nanotomography (Voxel resolution: 8.5 nm × 10.8 nm × 33 nm / 35,000× mag). a) original gray scale image. b) Gray-scale coded image illustrating the pore size distribution in a. The corresponding PSD curves determined in 2D- and in 3D-space are shown in Fig. 8.

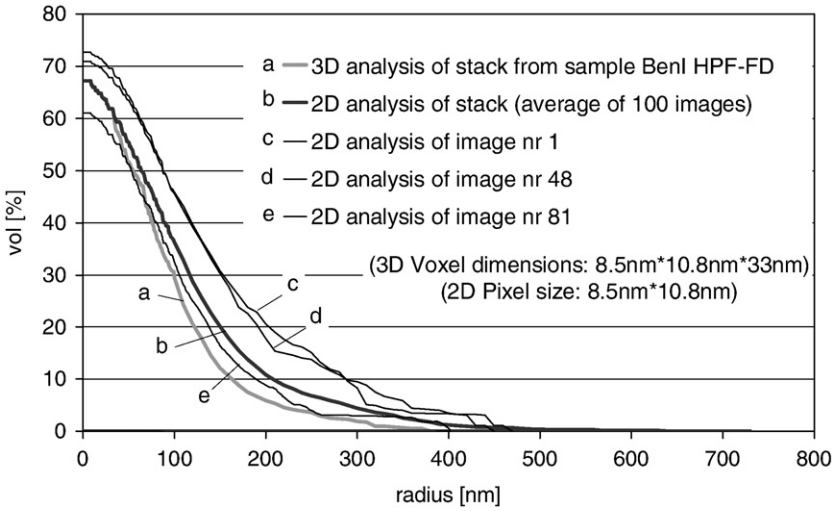

Fig. 8. Pore size distribution curves obtained from FIB-nt analysis of high pressure frozen, freeze dried and impregnated sample Ben I HPF–FD (see Fig. 7). Note that the pore radii obtained from the 3D-pore structure are nearly identical, but systematically smaller than those extracted from the individual 2D-images.

into the sectioned area may be larger or smaller than the 'true pore size', depending on the orientation of the section. As shown in Fig. 8, the difference between the 3D- and 2D-analyses is quite small, which indicates that the probability for both cases may be similar and therefore the different effects of both cases nearly cancel out. This is consistent with other studies of porous materials such as cement paste and fuel cell electrodes, where only very small differences are observed between 3D- and 2D-analyses of continuous PSDs (e.g. Holzer et al., 2009 and unpubl. data).

Overall, it can be concluded from this example that the delicate card house-like texture of Ben I which is preserved with high pressure freezing can be stabilized by means of controlled freeze drying and with careful impregnation procedures.

4.1.5. Comparison of all PSD curves for Ben I

A compilation of all previously discussed PSDs from Ben I is shown in Fig. 9. We first compare the eight PSD curves from the high pressure frozen samples (HPF). They all show total pore volume fractions between 60 and 70% which is roughly 10% lower than the estimated amount of free water in Ben I. Since the flaky clay particles are very thin (only a few pixels), slightly different threshold values for segmentation can easily lead to a shift of a few vol.%. This uncertainty may explain the observed underestimation of the pore volume fractions. Nevertheless, all 8 PSDs from HPF samples give similar porosities which indicate that the methodological reproducibility is satisfying. Furthermore, all 8 PSDs from HPF samples give a consistent picture of the size distributions. Thereby the majority of pores are in the range between 50 and 250 nm. However, at a closer look, slight but systematic variations can be recognized between freeze fractured and freeze dried HPF samples. The PSDs from the freeze dried sample (HPF–FD, blue and red curves) are systematically smaller than the PSDs from the freeze-fractured sample (HPF–FF, green curves). These deviations could indicate that slight structural reorganizations of the clay particles took place during freeze drying and subsequent infiltration with resin.

We are now including the PSDs from oven dried and plunge freeze dried samples in our comparison (see Fig. 9). Thereby, it becomes obvious that the above discussed deviations among the 8 PSDs from HPF samples are relatively small. Much larger deviations result from the artifacts which are produced by oven drying and plunge freeze

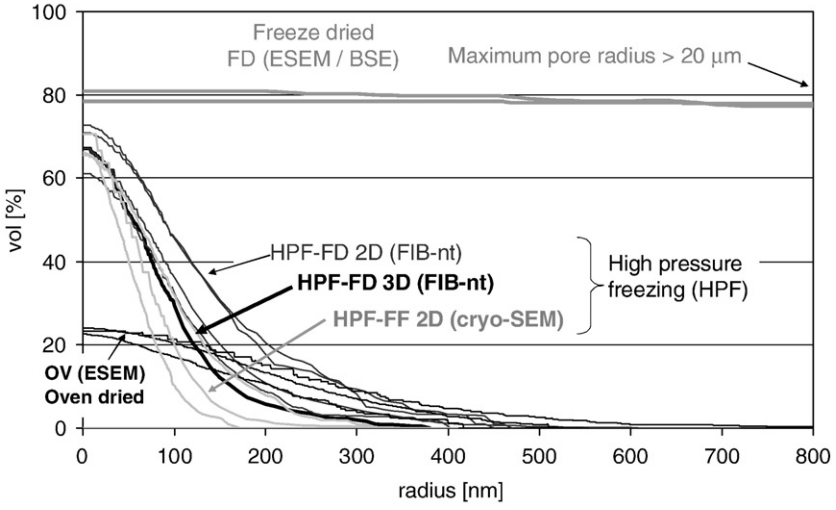

Fig. 9. Compilation of PSD data from Ben I (see Figs. 2, 4, 5, 8) showing large differences of the four sample preparation techniques. The initial pore structure is best preserved with high pressure freezing techniques. Plunge freezing leads to segregation artifacts (large ice crystals). Oven dried samples undergo drying shrinkage (small pore volume). FD = freeze dried, OV = oven dried, HPF–FD = high pressure frozen and freeze dried, HPF–FF = high pressure frozen and freeze fractured.

drying. Oven drying leads to considerable shrinkage, whereby the total pore volume fraction has decreased to only 25% in Ben I OV. In the plunge freeze dried sample Ben I FD, the initial pore volume is preserved (80 vol.%). However, growth of large ice crystals leads to a complete destruction of the delicate card house-type microstructure in Ben I. As a result of the freezing artifacts large pores with dimensions up to 20 µm have formed in Ben I FD which are representing the size of the former ice crystals.

Overall, the above results clearly indicate that plunge freezing with subsequent freeze drying as well as simple oven drying are not suitable methods for preparation of hydrated samples which contain free water. In contrast, even delicate card house structures as those observed in Ben I with 70 vol.% of free water can be preserved with the high pressure freezing methods.

4.2. Microstructure of the compacted sample Ben IV

Since the investigations of Ben I have shown that high pressure freezing is the most promising method for artifact-free sample preparation of hydrated bentonite, Ben IV is investigated exclusively with HPF methods. Ben IV is a compacted bentonite with a dry density of 1.55 kg/m^3. After saturation the sample should contain very little free water and it is assumed that the corresponding meso- and macropores do not form a percolating pore network.

The microstructure of the freeze-fractured sample Ben IV HPF–FF is shown in Fig. 10. In cryo-SEM, the compacted sample exhibits a very dense matrix, whereby the flaky morphology of the clay particles is the dominant microstructural feature. Unfortunately, the locations of free water cannot be detected easily, because in cryo-SEM the fractured surface is coated with a W-layer and therefore hardly any material contrast can be detected between frozen water and the clay matrix. In contrast, the fractured surface of Ben I exhibits a certain topography which allows the distinction of flaky clay particles from the surrounding matrix with frozen water. In Ben IV there are only a few pores and these pores cannot be distinguished from irregularities in the topography of the fractured surface. In order to detect the pores filled with free water, we have performed in-situ sublimation experiments within the sample chamber of the cryo-SEM. When the temperature is increased from −130 °C to −70 °C, the equilibrium vapour pressure rises from 10^{-6} mbar to 4×10^{-3} mbar and hence the free water at the sample surface starts sublimating in the microscope high vacuum chamber. An example of an in-situ sublimation experiment is illustrated in Fig. 10. The images on the left side represent the fracture surface before sublimation and those on the right side after sublimation. At higher magnifications it is clearly visible that small holes have formed locally (bottom right), whereas the surrounding clay matrix remains stable without any drying shrinkage. The newly formed holes are thus interpreted as mesopores from which free water is removed by sublimation. Unfortunately, these pores do not exhibit a distinct material contrast with the clay matrix. Therefore, it is not possible to extract a quantitative analysis of the pore structure from the cryo-SEM images.

After freeze drying and impregnation, the high pressure frozen material Ben IV HPF–FD can be sectioned with focused ion beam. Selected images from serial sectioning with FIB-nt are shown in Fig. 11 and a compilation of 3D data from FIB is given in Table 2. In the BSE gray scale images (upper row) the mesopores are visible. These mesopores form isolated sheets between the compacted clay particles which form a dense matrix. After binarization into pore and solid material (middle row) the size distribution of the mesopores can be calculated (bottom row). It has to be mentioned that the resolution of FIB/SEM is not sufficient to resolve the micro- and nanopores of the hydrated bentonite. Subsequent 3D-visualizations and PSD measurements are thus restricted to the coarser pores with radii larger than 15 nm, which host most of the free water.

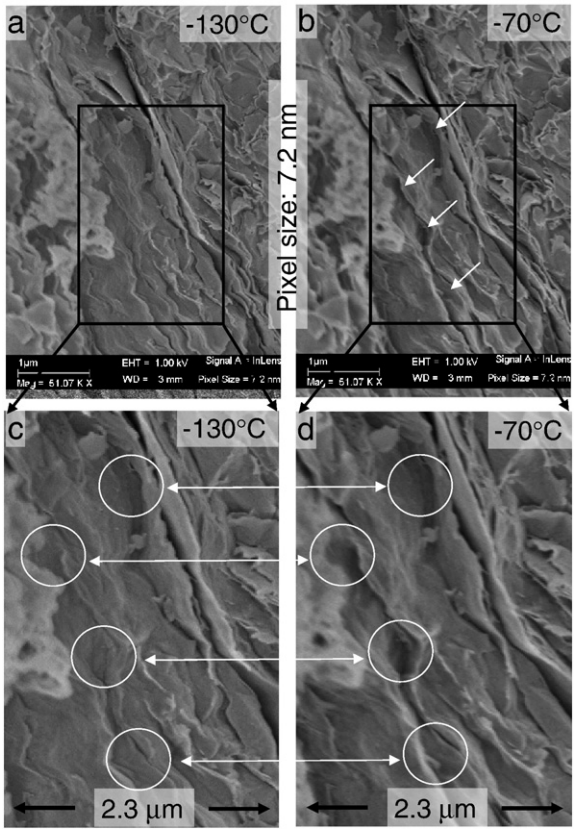

Fig. 10. Cryo-SEM images of high pressure frozen and freeze-fractured sample Ben IV HPF–FF. Comparison of fracture surfaces before (a and c) and after sublimation of free water (b and d) reveals the location of mesoscale pores. The images on the left side (a and c) show the initial topography of the freeze-fractured surface at −130 °C. At these temperatures frozen water is stable in high vacuum (10^{-6} mbar). In b and d, small holes have formed due to sublimation of free water from the pores. In-situ sublimation is achieved by increasing the temperature to −70 °C (vapour pressure: 4×10^{-3} mbar).

3D-reconstructions of the pore structure in Ben IV HPF–FD are shown in Fig. 12. The microstructure is best visible after triangulation of the pore surfaces (bottom right, solid material = transparent). The mesopores form isolated bodies with sheet-like morphology. It can be suggested that these mesopores with the free water are connected with each other only via the non-visible nano- and micropores along the particle surfaces and through the clay interlayers.

The continuous pore size distributions of Ben IV HPF–FD are measured from the 3D-pore structure and also in 2D from the single images of the FIB-stack (Fig. 13). The measured pore radii in the continuous PSD are dominated by the shortest distance to the pore wall at any point on the pore skeleton. Due to the sheet-like pore morphology, the shortest distances are very small. The majority of the measured pore radii are smaller than 50 nm. The maximum pore size is 91 nm in 3D and 110 nm in 2D. Very little differences are recognized between the PSD curves from 2D- and from 3D-analyses. As observed previously slightly larger pores are measured in 2D-analyses because the shortest pore distance may be hidden in the third dimension. However, the small difference indicates that pore size measurements from 2D imaging methods (SEM or TEM) are comparable in a first approximation with those from true 3D pore structures.

5. Discussion

Artifact-free sample preparation is the basis for reliable characterization of the pore structure in materials with swelling clays. In this study, four different sample preparation techniques were tested. From

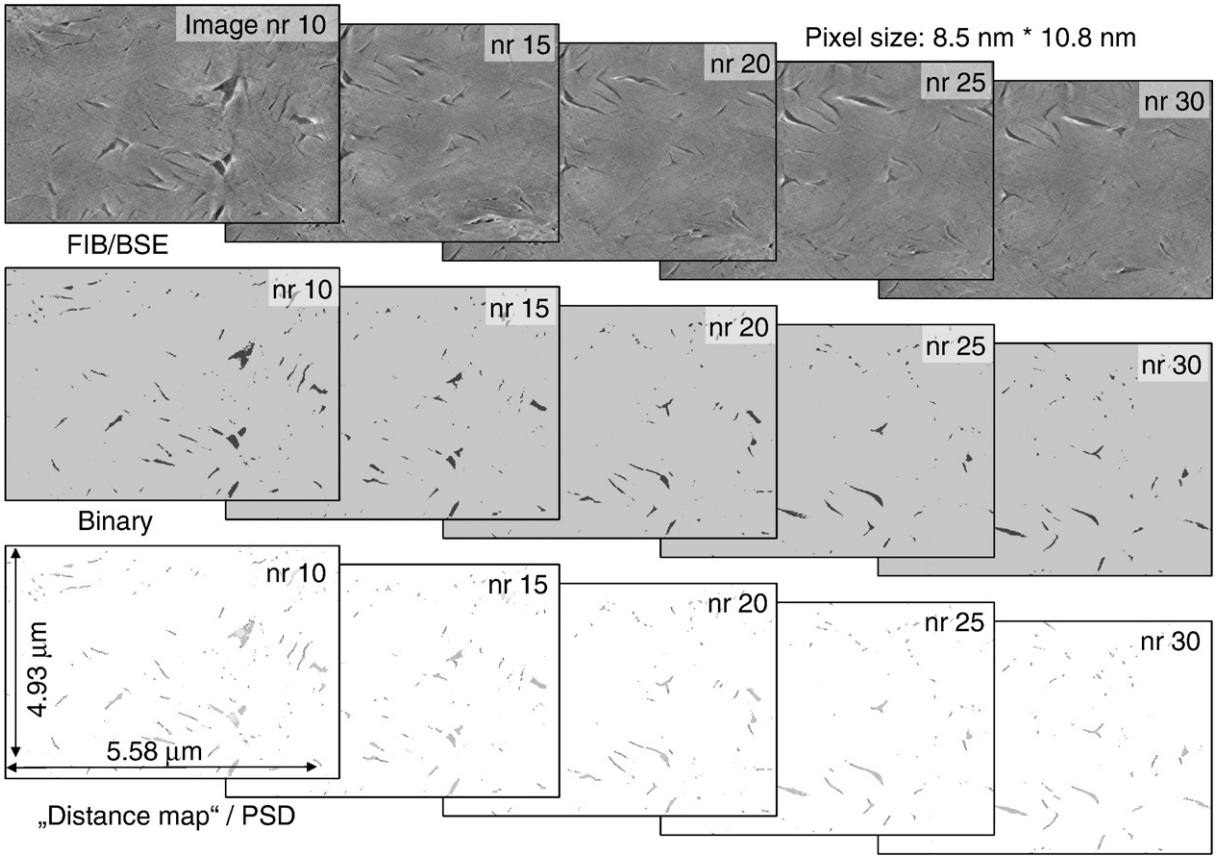

Fig. 11. Serial sectioning with FIB-nt of sample Ben IV HPF–FD after high pressure freezing and freeze drying. Every 5th image between layer numbers 10 and 30 is shown. The interlayer-distance is 25 nm. Upper row: BSE gray scale images after background levelling and filtering of waterfall-stripes. Middle row: binarization of pores and solid material. Bottom row: gray-scale coded map reflecting the continuous pore size distributions.

the investigation of the water-rich sample Ben I it can be concluded that oven drying and plunge freeze drying are not suitable for sample preparation of hydrated bentonite because they lead to drying shrinkage or to freeze segregation, respectively. The results from Ben I further indicate that preparation artifacts can be suppressed with high pressure freezing.

The high pressure freezing technique was then applied to the hydrated bentonite material Ben IV which represents similar material as the one which is used for engineered barrier systems in radioactive waste disposals. Quantitative descriptions of the pore structure in such compacted and hydrated bentonite are of major interest in the context of long-term predictions for radionuclide migration. Thereby, it is well known that diffusion in mesopores with free water is much faster than in the nanopores where chemical migration rates are reduced due to chemi- and physisorption. In the high pressure frozen bentonite Ben IV the mesopores can be visualized in 3D by means of FIB-nt. As can be seen in Fig. 12 the mesopores do not form a continuous pore network since they only represent 1.5 vol.%. The numerous small pores are almost uniformly dispersed over the bentonite microstructure. The distance between the individual mesopores is very small,—typically less than 1 µm. Consequently, transport of chemical species over meso- and macroscale distances cannot take place exclusively through the free water in the mesopores. The transport between the isolated mesopores has to be bridged via connections of nanopores which are hosted either between the clay particles or within the clay interlayers.

Continuous PSDs can be extracted with a high reproducibility from the FIB-nt analyses of high pressure frozen samples (Figs. 9 and 13). Nevertheless, for a validation of the measured PSDs a comparison with other characterization techniques such as mercury intrusion porosimetry (MIP) and BET is required. Very often MIP and BET are performed in combination with conventional sample preparation techniques such as oven drying or freeze drying. However, it was shown that these preparation techniques induce considerable artifacts and therefore the MIP- and BET-measurements of hydrated bentonite must be interpreted with caution. Nevertheless, a consistent picture of the pore structure in hydrated clay samples can only be obtained when the different porosimetry techniques are applied to samples which are treated with the same preparation technique. Thereby, for water-rich clay samples, high pressure freezing is the most suitable method. Unfortunately, the sample size in high pressure freezing is very limited (thickness<0.4 mm) because of the high heat

Table 2
Dimensions of 3D FIB-data.

Sample	Mag $10^3\times$	Nr of slices (*Z*-dir.)	Voxel dimensions				Voxel matrix (ROI)				Dimensions of data volume			
			X [nm]	*Y* [nm]	*Z* [nm]	Ø size [nm]	*X* [–]	*Y* [–]	*Z* [–]	Total [10^6]	*X* [µm]	*Y* [µm]	*Z* [µm]	Total [µm^3]
Ben I	35	100	8.48	10.76	33.00	14.44	300	500	100	15.00	2.54	5.38	3.30	45.17
Ben IV	35	200	8.48	10.76	25.00	13.16	658	458	200	60.27	5.58	4.93	5.00	137.49

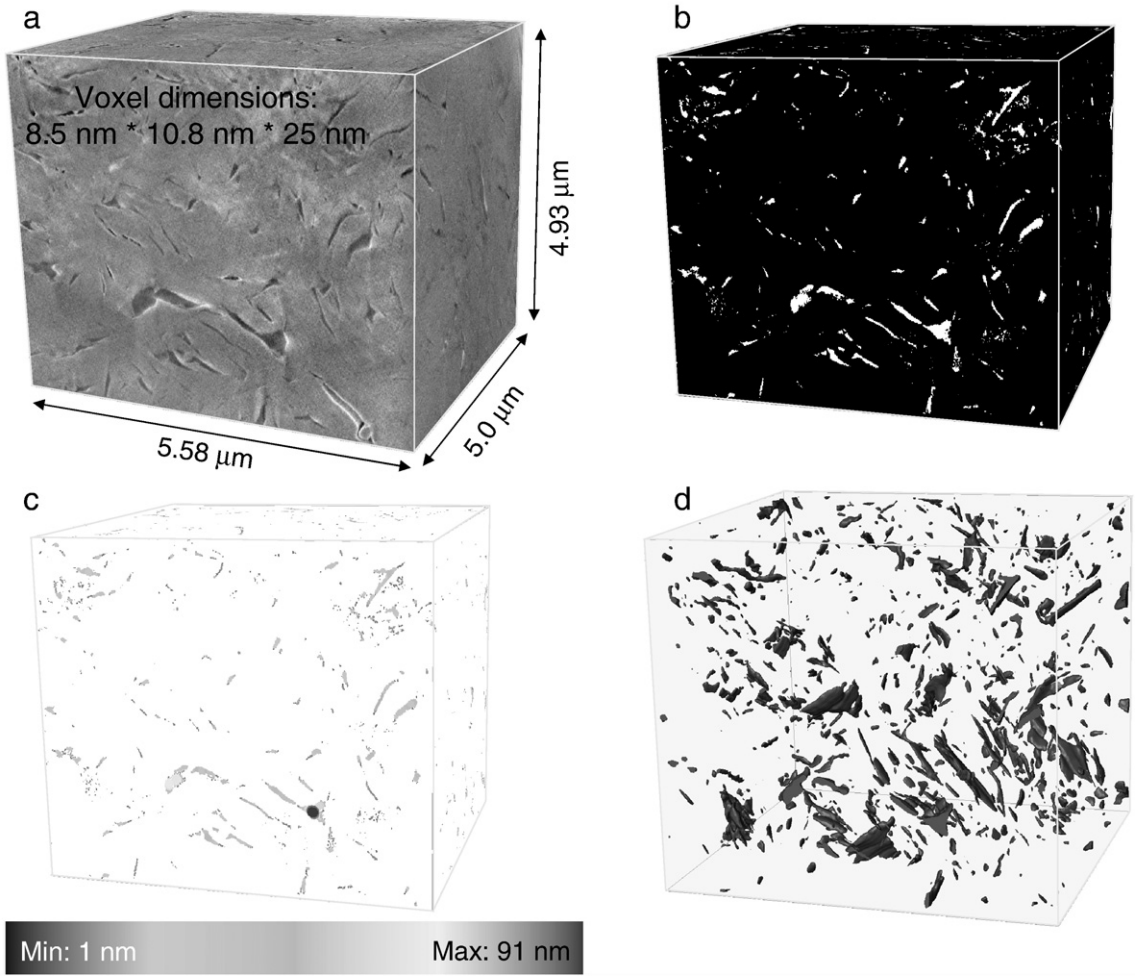

Fig. 12. 3D-reconstructions of FIB-nt data from sample Ben IV HPF–FD after high pressure freezing and freeze drying. a) Gray scale images after background levelling and filtering of waterfall-stripes, b) binarization into pore and solid phases, c) gray-scale coding of pore radii, d) triangulated pore surfaces (solid phase is transparent). Note that the pore objects are forming isolated sheets within the dense clay matrix.

capacity and the low thermal conductivity of water. Therefore, these samples are too small for reliable MIP- and BET analyses. For future investigations, the improvement of high pressure freezing devices which allow the preparation of larger samples will open new possibilities for combined pore size measurements with MIP, BET, FIB-nt, cryo-SEM and TEM.

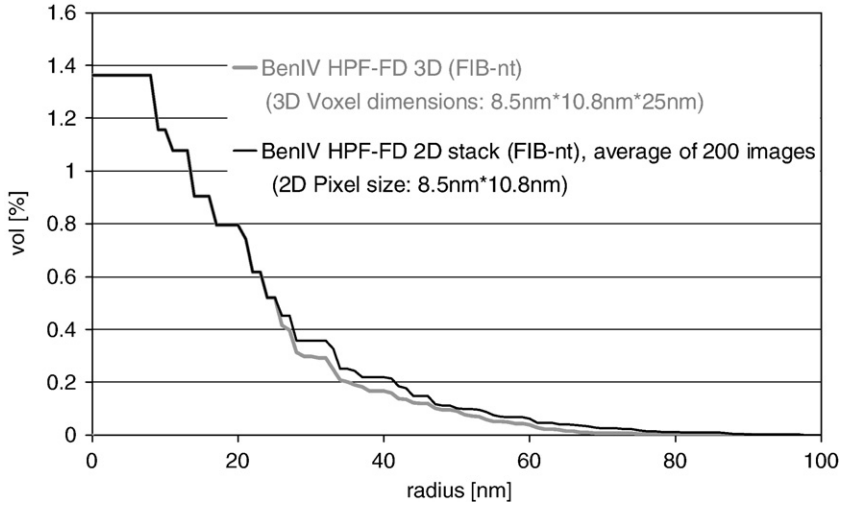

Fig. 13. Cumulative pore size distributions from high pressure frozen and freeze dried sample Ben IV HPF–FD (see Figs. 11 and 12). Black curve = 2D analysis: average of 200 PSDs acquired from each image in the FIB-stack. Gray curve = 3D-analysis from the same FIB-nt data volume. Note that the PSDs from 2D and 3D analyses are nearly identical, although the maximum pore size measured in 2D (110 nm) is larger than in 3D (91 nm).

6. Conclusions

In this study, it was shown that high pressure freezing and freeze substitution are well suitable as preparation techniques for microstructural investigations of hydrated bentonite. The high pressure frozen samples can be investigated after freeze fracturing by cryo-SEM or after controlled freeze drying and impregnation with FIB-nt and/or SEM. From the electron micrographs continuous PSDs can be extracted which give similar information as mercury intrusion porosimetry. For the bentonite samples the continuous PSDs from 2D- and from 3D-data are very similar. This indicates that the continuous PSDs extracted from SEM imaging are comparable with those from FIB-nt, which is not the case for conventional (discrete) PSD algorithms. Furthermore, the high resolution FIB-nt gives additional information about the three dimensional distribution of the mesopores and their connectivity. For the compacted bentonite with a dry density of 1.58 kg/m^3 it is shown that the mesopores (1.5 vol.%) do not form a continuously interconnected pore network. Transport of dissolved radionuclides can thus not entirely take place by diffusion in the free water of the mesopores. For the transport over distances above the micrometer-scale the pathways between the mesopores have to be bridged by nanopores in the interlayers or via the external double diffuse layers.

For a more complete characterization of the pore structure in hydrated bentonites, different length scales (nano–micro–meso) have to be probed and described quantitatively by means of correlative microscopy with SEM, FIB-nt, TEM and AFM but also with experimental techniques. In order to obtain internally consistent data the different analyses should be performed with identical samples. For this purpose it is necessary that the high pressure freezing technique is further improved so that also larger sample volumes can be prepared. These larger samples are required for representative experimental characterization (e.g. MIP and BET).

References

Appelo, C.A.J., 2008. A review of porosity and diffusion in bentonite. Technical report Nr. 08-4. POSIVA, Helsinki.

Bachmann, L., Mayer, E., 1987. Physics of water and ice: implications for cryofixation. In: Steinbrecht, R.A., Zierold, K. (Eds.), Cryotechniques in Biological Electron Microscopy. Springer, Berlin.

Biel, S.S., Kawaschinski, K., Wittern, K.-P., Hintze, U., Wepf, R., 2003. From tissue to cellular ultrastructure: closing the gap between micro- and nanostructural imaging. Journal of Microscopy 212, 91–99.

Chenu, C., Tessier, D., 1995. Low temperature scanning electron microscopy of clay and organic constituents and their relevance to soil microstructures. Scanning Microscopy 9, 989–1010.

Crumbie, A.K., 2001. SEM microstructural studies of cementitious materials: Sample preparation of polished sections and microstructural observations with backscattered images — artifacts and practical considerations. In: Jany, L.A., Nisperos, A.G. (Eds.), Proc. 23rd Int. Conf. on Cement Micr. ICMA, Albuquerque, USA, pp. 320–341.

Delage, P., Tessier, D., Marcel-Audiguier, M., 1982. Use of the Cryoscan apparatus for observation of freeze-fractured planes of a sensitive Quebec clay in scanning electron microscopy. Canadian Geotechnical Journal 19, 111–114.

Delage, P., Marcial, D., Cui, Y.J., Ruiz, X., 2006. Ageing effects in a compacted bentonite: a microstructure approach. Geotechnique 56, 291–304.

Gimmi, T., 2003. Porosity, pore structure and energy state of pore water of opalinus clay from Benken. Technical report NIB 03-09. Nagra, Wettingen, Switzerland.

Holzapfel, C., Schaef, W., Marx, M., Vehoff, H., Muecklich, F., 2007. Interaction of cracks with precipitates and grain boundaries: understanding crack growth mechanisms through focused ion beam tomography. Scripta Materialia 56, 697–700.

Holzer, L., Indutnyi, F., Gasser, P., Münch, B., Wegmann, M., 2004. 3D analysis of porous $BaTiO_3$ ceramics using FIB nanotomography. Journal of Microscopy 216, 84–95.

Holzer, L., Gasser, P., Münch, B., 2006a. Quantification of capillary pores and Hadley grains in cement paste using FIB-nanotomography. In: Konsta-Gdoutos, M.S. (Ed.), Measuring, Monitoring and Modelling Concrete Properties. Springer, Dordrecht, NL, pp. 509–516.

Holzer, L., Muench, B., Leemann, A., Gasser, P., 2006b. Quantification of capillary porosity in cement paste using high resolution 3D-microscopy: potential and limitations of FIB-nanotomography. In: Marchand, J. (Ed.), Advances in Concrete through Science and Engineering. RILEM PRO 51, Quebec, Canada, p. 247.

Holzer, L., Münch, B., Wegmann, M., Flatt, R., Gasser, P., 2006c. FIB-Nanotomography of particulate systems — part I: particle shape and topology of interfaces. Journal of the American Ceramic Society 89, 2577–2585.

Holzer, L., Gasser, P., Kaech, A., Wegmann, M., Zingg, A., Wepf, R., Münch, B., 2007. Cryo-FIB-nanotomography for quantitative analysis of particle structures in cement suspensions. Journal of Microscopy 227, 216–228.

Holzer, L., Muench, B., Cantoni, M., 2009. 3D-microstructure analysis of solid oxide fuel cell (SOFC) anode. In: Abolhassani, S., et al. (Ed.), Interdisciplinary Symposium on 3D Microscopy SSOM, Interlaken Switzerland, pp. 40–42.

Inkson, B.J., Mulvihill, M., Möbus, G., 2001. 3D determination of grain shape in a FeAl-based nanocomposite by 3D FIB tomography. Scripta Materialia 45, 753–758.

Israelachvili, J., 1991. Intermolecular and surface forces. Academic Press, Elsevier, Amsterdam.

Ito, H., 2006. Compaction properties of granular bentonites. Applied Clay Science 31, 47–55.

Karnland, O., Olsson, S., Nilsson, U., 2006. Mineralogy and sealing properties of various bentonites and smectite-rich clay materials. Technical report TR-06-30. SKB Swedish Nuclear Fuel and Waste Management Co, Stockholm.

Konrad, J., Zaefferer, S., Raabe, D., 2006. Investigation of orientation gradients around a hard Laves particle in a warm-rolled Fe_3Al-based alloy using a 3D EBSD-FIB technique. Acta Materialia 54, 1369–1380.

Kubis, A.J., Shiflet, G.J., Dunn, D.N., Hull, R., 2004. Focused ion-beam tomography. Metallurgical and Materials Transactions A 35A, 1935–1943.

Lasagni, F., Lasagni, A., Holzapfel, C., Mücklich, F., Degischer, H.P., 2006. Three dimensional characterization of unmodified and Sr-modified Al–Si eutectics by FIB and FIB EDX Tomography. Advanced Engineering Materials 8, 719–723.

Lasagni, F., Lasagni, A., Engstler, M., Degischer, H.P., Mücklich, F., 2008. Nano-characterization of cast structures by FIB-tomography. Advanced Engineering Materials 10, 62–66.

Münch, B., Holzer, L., 2008. Contradicting geometrical concepts in pore size analysis attained with electron microscopy and mercury intrusion. Journal of the American Ceramic Society 91, 4059–4067.

Münch, B., Gasser, P., Flatt, R., Holzer, L., 2006. FIB-Nanotomography of particulate systems — part II: particle recognition and effect of boundary truncation. Journal of the American Ceramic Society 89, 2586–2595.

Peron, H., Hueckel, T., Laloui, L., 2007. An improved volume measurement for determining soil water retention curves. Geotechnical Testing Journal 30, 1–8.

Russ, J.C., 1999. The image processing handbook. CRC Press, Boca Raton, USA.

Saiyouri, N., Hicher, P.Y., Tessier, D., 2000. Microstructural approach and transfer water modelling in highly compacted unsaturated swelling clay. Mechanics of cohesive-frictional materials 5, 41–60.

Smart, R.St.C., Zbik, M., Morris, G.E., 2004. STIMAN observation of aggregate structure in clay flocculation. COM 2004. Hamilton, Ontario, Canada, pp. 215–228.

Uchic, M.D., Groeber, M.A., Dimiduk, D.M., Simmons, J.P., 2006. 3D microstructural characterization of nickel superalloys via serial-sectioning using a dual beam FIB-SEM. Scripta Materialia 55, 23–28.

Wepf, R., 2007. Zoom-in beyond light microscopy. GIT Imaging and Microscopy 9, 28–34.

Wilson, J.R., Kopsiriphat, W., Mendoza, R., Chen, H.Y., Hiller, J.M., Thornton, K., Voorhees, P.W., Adler, S.B., Barnett, S.A., 2006. Three-dimensional reconstruction of a solid-oxide fuel-cell anode. Nature Materials 5, 541–544.

Zaafarani, N., Raabe, D., Singh, R.N., Roters, F., Zaefferer, S., 2006. 3D investigation of the texture and microstructure below nanoindent in a Cu single crystal using 3D EBSD and plasticity finite element simulations. Acta Materialia 54, 1863–1876.

Zbik, M.S., Martens, W.N., Frost, R.L., Song, Y.-F., Chen, Y.-M., Chen, J.-H., 2008. Transmission X-ray Microscopy (TXM) reveals the nanostructure of a smectite gel. Langmuir 24, 8954–8958.